Experimental Investigation of a Close-coupled Atomizer Using the Phase Doppler Measurement Technique

N. Apell*, C. Tropea, I. V. Roisman, J. Hussong
Institute for Fluid Mechanics and Aerodynamics, Technische Universität Darmstadt,
Alarich-Weiss-Straße 10, 64287 Darmstadt, Hessen, Germany
*Corresponding author email: apell@sla.tu-darmstadt.de

Abstract
A common method for producing metal powders used for additive manufacturing is based on the atomization of a stream of molten metal by means of a high-pressure gas flow. In the present experimental study, the influence of the liquid mass flow rate on the atomization result has been investigated for a close-coupled atomizer operated with water and air as a substitute for molten metal and argon gas.
The phase Doppler measurement technique has been employed to measure local particle size and velocity distributions within the spray. The results indicate that the liquid mass flow rate is a sensitive parameter in determining the mean particle size as well as the width of the particle size distribution. Its influence appears to be strongest in the center of the spray. Here, a decrease in the liquid mass flow rate has been found to lead to a significant decrease in the arithmetic mean particle diameter and a considerably narrower particle diameter distribution.

Keywords
Additive manufacturing, close-coupled atomization, molten metal atomization, phase Doppler measurement technique

Introduction

Metal additive manufacturing techniques allow for the cost-effective production of complex and functional high-value components made from a variety of materials [1, 2]. Accompanying the rising economic significance of these techniques, an increase in the demand for high quality metal powders has arisen, making improvements in powder production in regards to quality, yield and cost necessary [3].
One widely employed method for producing metal powders characterized by a high degree of sphericity and chemical purity is based on the atomization of molten metals by means of a high-pressure gas flow [1]. Among the different configurations used for gas-driven atomization, close-coupled atomization (CCA) has been found to be particularly suited for producing a high yield of fine particles. This is due to the close proximity of the two interacting fluids [4] and, therefore, the effectiveness of the energy transfer [5].
A typical close-coupled atomizer is schematically depicted in Figure 1a. Here, a stream of molten metal, which is either solely gravity-driven or additionally pressurized, is fed through a central liquid nozzle. The opening of the liquid nozzle is surrounded by a coaxial gas nozzle, which is commonly designed as either a single annular slit nozzle or a circumferential array of several circular nozzles. In both cases, the gas nozzle can be shaped purely convergent or convergent-divergent, producing a subsonic, sonic or supersonic gas jet.
The characteristics of powders produced by means of close-coupled atomization depend on the geometry of the atomizer, the physical properties of both fluids — liquid and gas — as well as on operating parameters. However, neither the respective sensitivities nor a reliable methodology for optimization according to a particular cost function have been established, resulting in the present situation that adjustment of these parameters remains highly empirical. To illustrate the unique features of a close-coupled atomizer and, at the same time, to underline the challenges in developing appropriate atomization models, as compared with conventional two-fluid

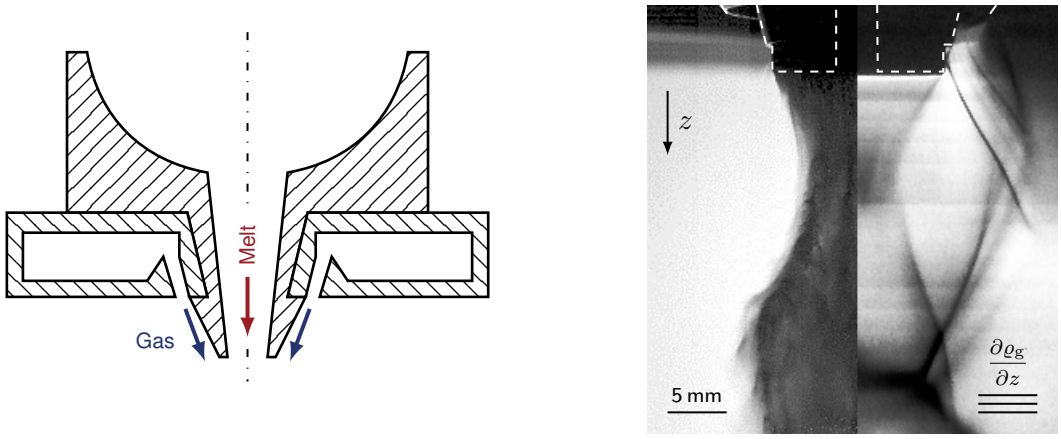

Figure 1. Close-coupled atomizer: a) schematic illustration of a typical configuration featuring a liquid as well as a gas nozzle in close proximity, and b) flow-field downstream of the atomizer for a gas stagnation pressure of $p_{t,g} \approx 1.6$ MPa visualized using high-speed imaging (left, multi-phase flow) and focusing Schlieren imaging (right, gas-only flow, as described by Luh et al. [6]).

atomizers, a composite image is presented in Figure 1b, the left half being a photograph of the liquid atomization and the right half showing a Schlieren image of the gas-only flow. Associated numerical simulations of the gas-only flow agree very well with the complex shock/expansion wave pattern depicted in the Schlieren image, as described by Luh et al. [6], and indicate that local Mach numbers of up to $Ma \approx 3.8$ are existent at these operating conditions. The present study has the aim of systematically investigating the influence of the liquid mass flow rate $\dot{m}_l$ on the atomization result and providing a deeper insight into causes of local variations of particle size and velocity within the spray.

Experimental Methods

To achieve this aim, an experimental study has been performed at laboratory scale. A brief overview of the experimental test rig as well as the measurement system is given below, with particular focus on the phase Doppler system used to measure particle size and velocity throughout the spray.

Laboratory Test Rig

The laboratory test rig has been built replicating one-to-one a close-coupled atomizer used in an existing metal powder production pilot plant. However, it is operated using water and air as a substitute for molten metal and argon gas. By carefully choosing physical fluid properties and operational parameters, most dimensionless numbers governing the atomization of molten metal can be matched in the laboratory experiments. Consequently, this approach allows for an easier accessibility for measurement techniques than on a test rig operating with molten metal. For instance, while for molten metal the mass flow rate can usually only be approximated as a time average for a known batch size and atomization duration [7], here the instantaneous flow rate of water is readily available and can be carefully controlled.

Water is supplied to the atomizer by means of a pressure vessel having a volume of 42 dm^3. This allows for adjusting the liquid mass flow rate $\dot{m}_l$ independently from the gas flow by freely varying the applied overpressure Δp_l ranging from 0 MPa to 1 MPa. Additionally, the pressure vessel features a heating system, which enables heating the water to a temperature of up to $T_l = 85$ °C and, therefore, adjusting its physical properties, mainly its dynamic viscosity μ_l. As a result, this allows variation of the Ohnesorge number Oh over a range of approximately 2.5:1, making it possible to investigate the influence of this dimensionless number on the atomization result. For the present study, only results obtained using water at ambient temperature will be

presented, since the dependence on Ohnesorge number Oh has been found to be small.
The gas supply line provides access to about $18\,\mathrm{m}^3$ of compressed air and the maximum available pressure is $3.5\,\mathrm{MPa}$. The gas nozzle is designed as a single annular slit nozzle with a convergent-divergent shape resulting in an exit Mach number of $Ma = 1.2$. During the atomization, it is operated with a gas stagnation pressure $p_{\mathrm{t,g}}$ ranging from $0.6\,\mathrm{MPa}$ to $2.1\,\mathrm{MPa}$ and the backpressure is equal to the ambient pressure p_{a}. Thus, the flow is perfectly expanded for a gas stagnation pressure of approximately $p_{\mathrm{t,g}} = 0.25\,\mathrm{MPa}$. However, since the defined operational range starts at a gas stagnation pressure of $p_{\mathrm{t,g}} = 0.6\,\mathrm{MPa}$, the flow is underexpanded in the entire operational range and the flow field downstream of the atomizer is characterized by the complex interaction of Prandtl-Meyer expansion waves and shocks. For the present atomizer, an experimental and numerical investigation of the flow field has been performed by Luh et al. [6] for gas-only flow and by Vogl et al. [8] for the two-phase flow, exhibiting excellent qualitative agreement.

Phase Doppler Measurement System

In order to measure particle size and velocity distributions in the atomized spray for different set points of operation, the test rig is equipped with a Dantec Dynamics dual-mode phase Doppler system. This system comprises a FlowExplorer DPSS laser transmitter featuring two wavelengths, a HiDense probe receiver, a Dual PDA detector unit as well as an upgraded BSA P60 flow and particle processor. Additionally, transmitter and receiver are mounted on a traverse system, which allows for exact positioning of the measurement volume within the spray.

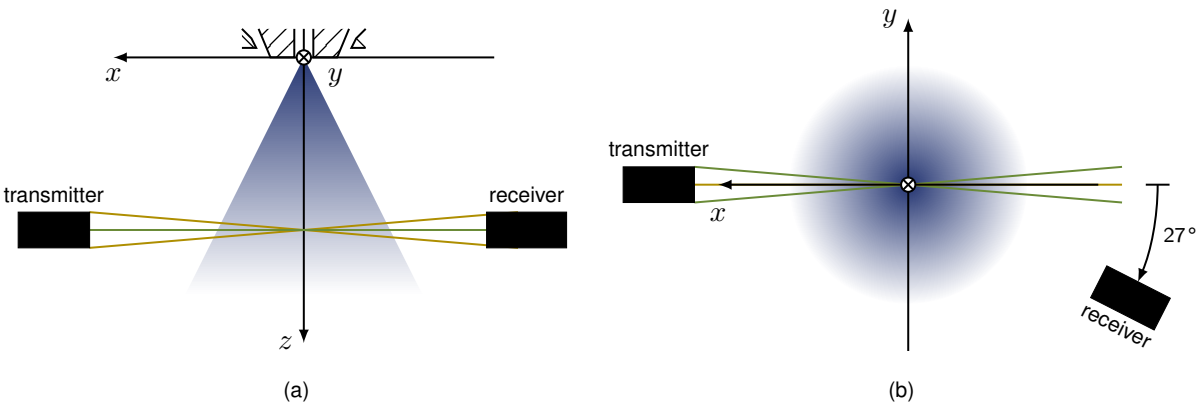

Figure 2. Schematic illustrations of the geometric arrangement of the phase Doppler setup: a) side view, and b) top view.

In Figure 2 schematic illustrations of the geometric arrangement of the phase Doppler system as well as the defined Cartesian coordinate system are depicted. The dual-mode configuration combines a standard and a planar phase Doppler system, which allows for measuring components of the particle velocity in the z-direction and the y-direction, u_z and u_y, respectively. Additionally, this provides means for validating the sphericity of the detected particles, as described by Tropea et al. [9].
The current optical configuration is suited for measuring particles having a diameter d of up to $107\,\mu\mathrm{m}$, a velocity in z-direction u_z in the range from $-94\,\mathrm{m\,s}^{-1}$ to $486\,\mathrm{m\,s}^{-1}$ and a velocity in y-direction u_y ranging from $-200\,\mathrm{m\,s}^{-1}$ to $200\,\mathrm{m\,s}^{-1}$. As a result, in the present study, the system has achieved an average validation rate of $84\,\%$ and an average spherical validation rate of $70\,\%$, which is deemed to be acceptable considering the extreme flow conditions.
For each measurement position, $35\,000$ particles have been validated, resulting in a statistically sufficient data basis. That is, typical statistics describing the particle size and velocity distribution have been found to converge satisfactorily within $15\,000$ validated particles.
In order to account for the bias introduced by the laser and phase Doppler measurement prin-

ciple, the raw data is corrected in two ways. The correlation between particle velocity and data rate is taken into account by applying a transit time weighting scheme introduced by Hoesel and Rodi [10]. Additionally, the correlation between particle size and data rate is accounted for by performing a probe volume correction described by Widmann [11] and based on an estimator of the detection volume given by Albrecht et al. [12]. As an additional means of assessing the statistical error of the results, non-normal 95 % confidence intervals are estimated for all calculated statistics employing a non-parametric bootstrap algorithm based on 10 000 re-sampled distributions each, as described by Efron and Tibshirani [13].

Results and Discussion

In the following, the results of phase Doppler measurements in a plane located 500 mm downstream of the liquid nozzle will be presented. The spray is assumed to be rotationally symmetric about the z-axis and the radial distribution of its properties is characterized by data along the negative y-axis (see Figure 2). In this way, the adverse effects of obscuration on the data quality are minimized and the third component of the particle velocity, which cannot be measured, is assumed to be sufficiently small.

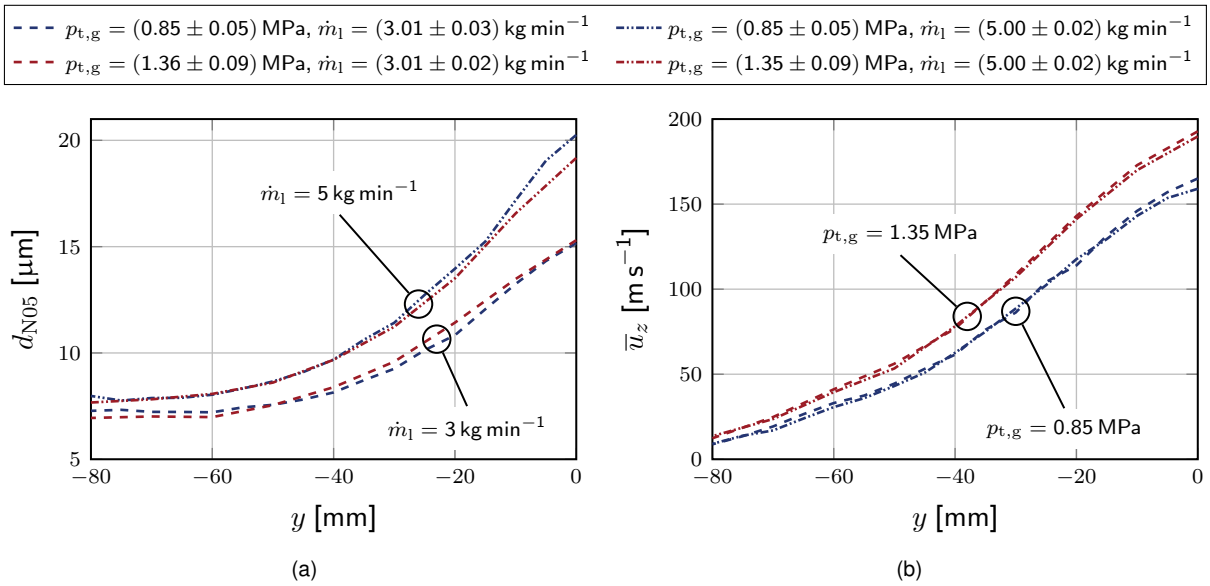

Figure 3. Distribution of particle statistics along the y-axis for different gas stagnation pressures $p_{t,g}$ and liquid mass flow rates $\dot{m}_l$ ($x = 0$ mm, $z = 500$ mm): a) arithmetic mean diameter d_{10}, and b) arithmetic mean velocity in z-direction $\overline{u}_z$. 95 % confidence intervals are not shown due to being similar in size to the line width.

In Figure 3a the arithmetic mean diameter d_{10} of particles in the spray is shown as a function of the y-coordinate for four different set points of operation, including two different gas stagnation pressures $p_{t,g}$ and two different liquid mass flow rates $\dot{m}_l$. Here, as well as in the following, the set point of operation is reported as the mean value and 1.96 times the standard deviation (95 % confidence interval under the assumption of normality). The results indicate that the largest particles accumulate in the center of the spray, while the arithmetic mean diameter d_{10} decreases with increasing distance from the center. Furthermore, the particle size in the center of the spray appears to be more sensitive to changes of the set point of operation. More specifically, a decrease in the liquid mass flow rate $\dot{m}_l$ leads to smaller arithmetic mean diameters d_{10}. On the other hand, the influence of the gas stagnation pressure $p_{t,g}$ appears to be less significant, at least for the set points of operation considered here. Finally, with regard to the smaller particles farther removed from the center of the spray, the presented results suggest that a lower limit for the arithmetic mean diameter d_{10} exists, which is virtually insensitive to the set points of operation investigated in this study.

In Figure 3b the mean particle velocity in the z-direction $\overline{u}_z$ is shown as a function of the y-

coordinate. As can be seen, the influence of the liquid mass flow rate $\dot{m}_\text{l}$ on the mean particle velocity in z-direction $\overline{u}_z$ is rather small. However, it can also be noted that the fastest particles accumulate in the center of the spray and that the velocity quickly decays with increasing distance from the center. The particle velocity in the y-direction u_y is not presented in this study, since it is almost two orders of magnitude smaller than the velocity in the z-direction u_z.

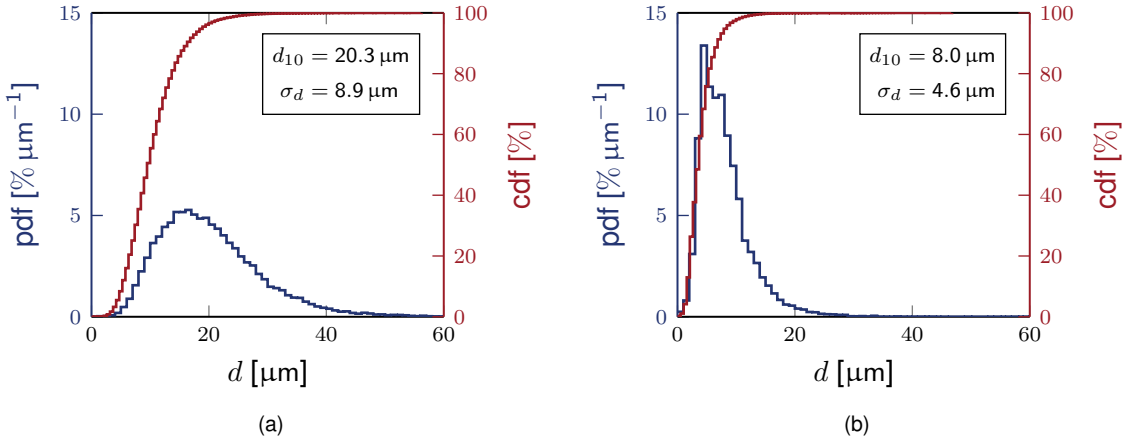

Figure 4. Particle diameter distributions for a gas stagnation pressure of $p_{\text{t,g}} = (0.85 \pm 0.05)$ MPa and a liquid mass flow rate of $\dot{m}_\text{l} = (5.00 \pm 0.02)\,\text{kg min}^{-1}$ at two selected positions along the y-axis ($x = 0$ mm, $z = 500$ mm): a) $y = 0$ mm, and b) $y = -60$ mm.

In order to illustrate the influence of the radial position within the spray on the dispersion of the particle size, in Figure 4 particle diameter distributions are shown as discrete probability density functions (pdf) as well as discrete cumulative distribution functions (cdf) at two different measurement positions along the y-axis. Additionally, the arithmetic mean diameter d_{10} as well as the diameter standard deviation σ_d are depicted inside of the respective histogram. The set point of operation is characterized by a gas stagnation pressure of $p_{\text{t,g}} = (0.85 \pm 0.05)$ MPa and a liquid mass flow rate of $\dot{m}_\text{l} = (5.00 \pm 0.02)\,\text{kg min}^{-1}$ and the data are taken from the same sample as shown in Figure 3. As can be seen, the width of the particle diameter distribution decreases with increasing distance from the center of the spray. That is, the diameter standard deviation σ_d is reduced by 48 % when moving 60 mm radially outwards (see Figures 4a and 4b). Measurements at intermediate y-positions show that this variation in size and distribution width is monotonic. Since the center of the spray has been found to be more sensitive to changes in the liquid mass flow rate $\dot{m}_\text{l}$, in the following discussion, only this particular measurement position will be considered.

In Figure 5 particle size statistics are shown in dependence of the liquid mass flow rate $\dot{m}_\text{l}$ for three different constant gas stagnation pressures $p_{\text{t,g}}$. In particular, the liquid mass flow rate $\dot{m}_\text{l}$ has been reduced from 8 kg min^{-1} to 3 kg min^{-1} in constant steps of 1 kg min^{-1}. Here, as well as in Figure 6, the line corresponds to the mean value and the shaded area illustrates fluctuations as a 95 % confidence interval in both directions.

Results shown in Figure 5a indicate an almost linear relationship between the arithmetic mean diameter d_{10} and the liquid mass flow rate $\dot{m}_\text{l}$. That is, a decrease in the latter causes a decrease in the arithmetic mean diameter d_{10}, which, for the considered parameter range, has been found to be as large as 42 %. This behavior appears to be independent of the chosen gas stagnation pressure $p_{\text{t,g}}$. Moreover, the results also suggest that an increased gas stagnation pressure $p_{\text{t,g}}$ leads to a decreased arithmetic mean diameter d_{10}. However, since the here considered gas stagnation pressures $p_{\text{t,g}}$ only cover the lower half of the defined range, this trend remains a subject for further investigation.

As a measure of the dispersion of the particle size, the standard deviation of the particle diameter distribution σ_d is shown in Figure 5b. It appears that reducing the liquid mass flow rate $\dot{m}_\text{l}$ leads to a significantly narrower particle diameter distribution. Furthermore, at least for the

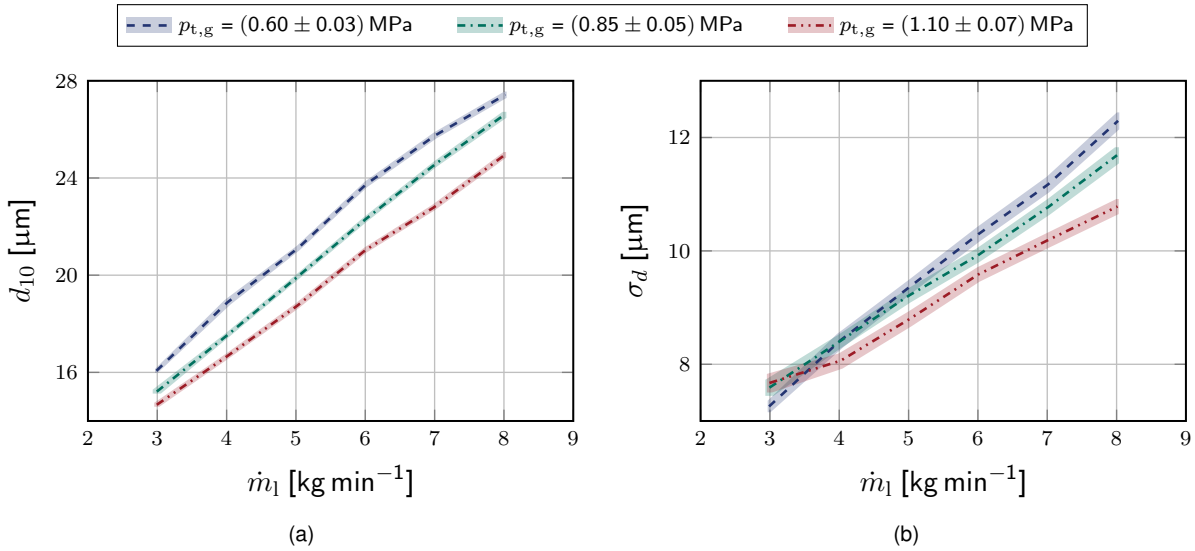

Figure 5. Particle size statistics in the center of the spray as a function of the liquid mass flow rate $\dot{m}_l$ for different constant gas stagnation pressures $p_{t,g}$ ($z = 500$ mm): a) arithmetic mean diameter d_{10}, and b) diameter standard deviation σ_d.

higher liquid mass flow rates $\dot{m}_l$ considered here, an increase of the gas stagnation pressure $p_{t,g}$ has a qualitatively similar effect. However, again, this still needs to be confirmed for the upper half of the defined parameter range.
An often considered operational parameter is the gas-to-liquid ratio GLR, which is defined as the ratio of the gas mass flow rate $\dot{m}_g$ and the liquid mass flow rate $\dot{m}_l$:

$$GLR = \frac{\dot{m}_g}{\dot{m}_l}. \tag{1}$$

As pointed out by Miller et al. [14], the gas-to-liquid ratio GLR can be understood as a first order measure of atomization efficiency. That is, for identical powder and particle characteristics, a lower gas-to-liquid ratio GLR is equivalent to a higher atomization efficiency.

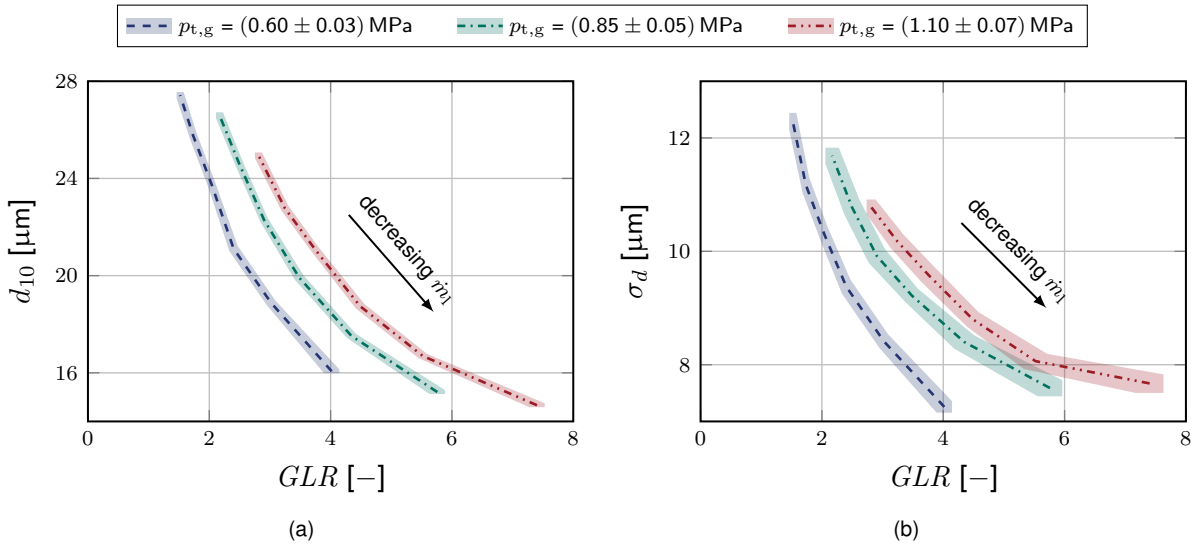

Figure 6. Particle size statistics in the center of the spray as a function of the gas-to-liquid ratio GLR for different constant gas stagnation pressures $p_{t,g}$ ($z = 500$ mm): a) arithmetic mean diameter d_{10}, and b) diameter standard deviation σ_d.

The same results, which have already been presented in Figure 5, are again shown in Figure 6, but as a function of the gas-to-liquid ratio GLR. Here, the arithmetic mean diameter d_{10} appears

to decrease with increasing gas-to-liquid ratio GLR (see Figure 6a). Additionally, the data suggests that a lower limit exists. A similar behavior has been observed by Ünal [15, 16] for the atomization of tin employing nitrogen gas. Furthermore, for a constant gas-to-liquid ratio GLR, different resulting arithmetic mean diameters d_{10} can be achieved, depending on the gas stagnation pressure $p_{\mathrm{t,g}}$. This has also been noted by Urionabarrenetxea Gomez et al. [17] in an experimental study atomizing a multitude of different metals and employing several different gases. Consequently, they have concluded that the gas-to-liquid ratio GLR, as a standalone parameter, does not take into account the gas flow field, in particular, the local gas velocity u_{g}. Figure 6b shows a similar behavior for the diameter standard deviation σ_d. It decreases with increasing gas-to-liquid ratio GLR, approaching a lower limit, and, for a constant gas-to-liquid ratio GLR, varies as a function of the gas stagnation pressure $p_{\mathrm{t,g}}$.

Summary and Conclusions

In the present study, the influence of the main operational parameters, including the liquid mass flow rate $\dot{m}_{\mathrm{l}}$ and the gas stagnation pressure $p_{\mathrm{t,g}}$, on the close-coupled atomization of water has been investigated experimentally. Phase Doppler measurements of particle size and velocity have been performed in a plane 500 mm downstream of the liquid nozzle, where the spray can be considered to be fully developed. The data have been analyzed in regards to the arithmetic mean particle diameter d_{10} as well as the width of the particle diameter distribution, characterized by its standard deviation σ_d.

The results indicate that, for a constant gas stagnation pressure $p_{\mathrm{t,g}}$, a decrease in the liquid mass flow rate $\dot{m}_{\mathrm{l}}$ not only significantly reduces the arithmetic mean diameter d_{10}, but also leads to a considerably narrower particle size distribution. However, with regard to the atomization efficiency, practical considerations in terms of the atomization process have to also be taken into account. Not only does a reduced liquid mass flow rate $\dot{m}_{\mathrm{l}}$ lead to a smaller yield of produced powder, but, as noted by Anderson et al. [18], it increases the risk of melt stream freeze-off. Consequently, a compromise between particle size, process stability and atomization efficiency has to be found.

Outlook

The result of the present study is a comprehensive set of particle size and velocity data obtained for well-defined set points of operation. Future work will focus on using this data for developing improved predictive models describing the mechanisms found in close-coupled atomization. Furthermore, the data will serve as a means for validating numerical simulations performed using identical boundary conditions.

Acknowledgements

The authors gratefully acknowledge the Indo-German Science & Technology Centre (IGSTC) for the financial support of the project “Metal Powder Production for Additive Manufacturing” (PPAM), funding code 01DQ19005A.

Nomenclature

μ_{l}	Liquid dynamic viscosity [Pa s]
ϱ_{g}	Gas density [kg m^{-3}]
σ_d	Standard deviation of the particle diameter distribution [m]
d	Particle diameter [m]
d_{10}	Arithmetic mean particle diameter [m]
GLR	Gas-to-liquid ratio [$-$]
Ma	Mach number [$-$]
$\dot{m}_{\mathrm{g}}$	Gas mass flow rate [kg s^{-1}]
$\dot{m}_{\mathrm{l}}$	Liquid mass flow rate [kg s^{-1}]

Oh Ohnesorge number [$-$]
p_{a} Ambient pressure [Pa]
$p_{\text{t,g}}$ Gas stagnation pressure [Pa]
Δp_{l} Liquid overpressure [Pa]
T_{l} Liquid temperature [℃]
u_{g} Gas velocity [m s^{-1}]
u_y Particle velocity in y-direction [m s^{-1}]
u_z Particle velocity in z-direction [m s^{-1}]
$\overline{u}_z$ Arithmetic mean particle velocity in z-direction [m s^{-1}]
x, y, z Cartesian coordinates [m]

References

[1] Yang, L., Hsu, K., Baughman, B., Godfrey, D., Medina, F., Menon, M., Wiener, S., 2017, Additive Manufacturing of Metals: The Technology, Materials, Design and Production, Springer Series in Advanced Manufacturing, Springer International Publishing, Cham.

[2] Milewski, J. O., 2017, Additive Manufacturing of Metals: From Fundamental Technology to Rocket Nozzles, Medical Implants, and Custom Jewelry, volume 258 of *Springer Series in Materials Science*, Springer International Publishing, Cham.

[3] Metal Powder Industries Federation, 2017, PM Industry Roadmap: Technology Update for the Powder Metallurgy Industry, Metal Powder Industries Federation, Princeton, New Jersey.

[4] Anderson, I. E., Terpstra, R. L., 2002, *Materials Science & Engineering A*, 326 (1) pp. 101–109.

[5] Heck, U., Fritsching, U., Bauckhage, K., 2000, *Atomization and Sprays*, 10 (1) pp. 25–46.

[6] Luh, M. F., Vogl, N., Odenthal, H.-J., V. Roisman, I., Tropea, C., 2018, in Proceedings of the 14th Triennial International Conference on Liquid Atomization and Spray Systems, ICLASS 2018.

[7] Allimant, A., Planche, M. P., Bailly, Y., Dembinski, L., Coddet, C., 2009, *Powder Technology*, 190 (1-2) pp. 79–83.

[8] Vogl, N., Odenthal, H.-J., Hüllen, M., Luh, M., Roisman, I., Tropea, C., 2019, in Proceedings of the 4th European Steel Technology and Application Days.

[9] Tropea, C., Xu, T.-H., Onofri, F., Géhan, G., Haugen, P., Stieglmeier, M., 1996, *Particle & Particle Systems Characterization*, 13 (2) pp. 165–170.

[10] Hoesel, W., Rodi, W., 1977, *Review of Scientific Instruments*, 48 (7) pp. 910–919.

[11] Widmann, J., Presser, C., Leigh, S., 2001, *Measurement Science and Technology*, 12 pp. 1180–1190.

[12] Albrecht, H.-E., Borys, M., Tropea, C., Damaschke, N., 2003, Laser Doppler and Phase Doppler Measurement Techniques, Experimental Fluid Mechanics, Springer, Berlin Heidelberg.

[13] Efron, B., Tibshirani, R., 1994, An Introduction to the Bootstrap, volume 57 of *Monographs on Statistics and Applied Probability*, Chapman & Hall, New York.

[14] Miller, R. S., Miller, S. A., Savkar, S. D., Mourer, D. P., 1996, *International Journal of Powder Metallurgy*, 32 (4) pp. 341–352.

[15] Ünal, R., 2007, *Powder Metallurgy*, 50 (1) pp. 66–71.

[16] Ünal, R., 2007, *Powder Metallurgy*, 50 (4) pp. 302–306.

[17] Urionabarrenetxea Gomez, E., Avello, A., Rivas, A., Martín, J. M., 2021, *Materials & Design*, 199 p. 109441.

[18] Anderson, I. E., Figliola, R. S., Morton, H., 1991, *Materials Science & Engineering A*, 148 (1) pp. 101–114.